Front. Optoelectron. China 2010, 3(2): 190–193
DOI 10.1007/s12200-010-0002-3

RESEARCH ARTICLE

Limit of accuracy in laser fabrication with metal powder

Xubao WANG (✉), Tiechuan ZUO

Institute of Laser Engineering, Beijing University of Technology, Beijing 100124, China

Abstract The research presented in this paper focuses on the laser-powder interaction. Through the experiment with metal powder in micrometers, we found that, in an invariable laser power density, the thickness of the final fabricated thin wall was similar to the geometrical dimension of the powder line, but could be much greater than the laser focus spot, even greater than two orders of magnitude. Furthermore, this paper showed that, the unmelted and semi-fused particles were concentrated. Thus, in this paper, combining the optical scattering theory with capillarity and infiltration theory pointed out the inducement effect of laser and the self-melting of powder. Based on the experimental phenomena and theory, we get our own ideas on the laser micro-fabrication.

Keywords laser-powder interaction, metal powder, scattering, capillary tube forces

1 Introduction

Rapid prototyping (RP) technology, also called layered manufacturing (LM) or solid freeform fabrication (SFF), produces physical objects additively layer-by-layer directly from computer-aided design (CAD) data. The first applications of SFF were in rapid prototyping, and a number of commercially successful proto-typing processes have been developed from SFF research (e.g., fused deposition modeling [1,2], selective laser sintering [3–7] and 3D printing [8]). Significant progress has also been made in applying SFF concepts to the automated manufacture of functional components or features of components out of metals. Many approaches involve the fabrication of a semi-porous part via SFF, followed by postprocessing such as infiltration by a low-melt alloy [7,9–13] or hot isostatic pressing [3,5]. Some of the most promising processes considered to date involve the direct fusion of metal powder by a moving laser (e.g., selective laser melting [14–18], laser-engineered net shaping (lens) [19,20] and direct metal deposition [21–25]).

Received August 31, 2009; accepted December 17, 2009

E-mail: wangxubao@bjut.edu.cn

2 Experiment and experimental phenomena

Using SFF processes for direct micro-manufacturing of metal parts, the machining accuracy is a fundamental question [4,6,16–18,20]. In order to find out the limit of accuracy, an experiment is accomplished by melting metal powder with the laser: melted a powder line by focused laser directly, a thin wall will be produced finally.

In fact, experimenting on the 2–3 μm iron powder with the 0.532 μm laser is to produce the thin wall under an argon atmosphere. For supplying laser power density of about 4.76×10^4 W/cm^2, the focusing diameter is about 50 μm, which was measured by a Beamcode SYS [26]. This intensity is a threshold value for melting. The line width of the accumulation joined by powder granules is about 130 μm. The laser scan speed is set up to 4 mm/s.

With this method, we gained a thin wall of 127 μm in 3 levels (as shown in Fig. 1). The average height of every level is about 0.3 mm. The cross section of the iron thin wall under an electronic microscope is shown in Fig. 1. The fracture analysis diagram is shown in Fig. 1(b); the left sections of both Figs. 1(a) and 1(b) are the tops of the thin wall, and the right sections of both are the bottoms.

It is interesting that a former experiment was done separately with a focus spot of 25 μm and 5.4 μm instead of 50 μm, and all of the other process parameters, including the laser power density 4.76×10^4 W/cm^2, line width of the powder accumulation 130 μm, scan speed 4 mm/s and layer thickness 0.3 mm, were kept unchanged, and the same final results of 127 μm were obtained.

Through 25 experimental times above in this way, we get that, in every process, 4.76×10^4 W/cm^2 is the minimum value for melting powder. However, the laser energy is different. That is to say that using different energy, the same parts come. Here, the power density of 4.76×10^4 W/cm^2 plays a fusee role in the process.

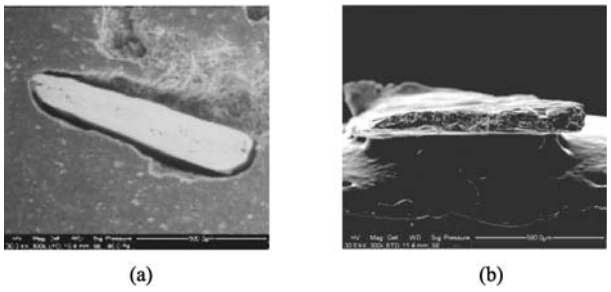

Fig. 1 Cross section of iron thin wall under an electronic microscope. (a) Macroscopic organization of iron wall cross section; (b) fracture analysis diagram

Observing the cross section of the iron wall through the electron microscope (as shown in Fig. 1), we find that there are some granules of which the size is similar to the original powder granules in the central section of the wall, and both sides along these granules are comparatively compact (as shown in Fig. 2).

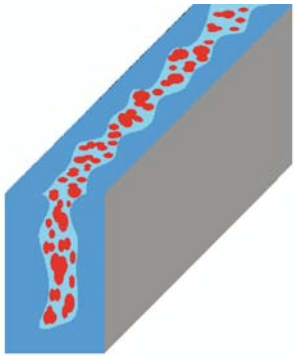

Fig. 2 Diagrammatic sketch of iron wall

3 Scattering of laser and self-melting of powder

As we all know, powder has relatively large specific surface area and surface energy and lacks the surface electron coordinate. Thus, compared to the macroscopic material of the same substance, it puts up a feature of low thermal conductivity. In the experiment, the photo of the still powder granules goes as Fig. 3 (but factually, the intervals in the granules are much greater). When the thermal conduction is omitted, the dimension of the final production does not relate to the focus spot but to the line width of the powder. The exact reason is that before the fusion of the powder, the laser scatters due to the granules' random arrangement. In the experiment, when the laser irradiates on the powder, its scattering is eligible for the Mie theory [27–33]. The dimension of the powder granule is similar to the laser wavelength.

Based on the Mie theory, when a parallel light with an intensity of I_0 irradiates on isotropic spherical granules, the scattered light intensity at x distance from the diffuser will be

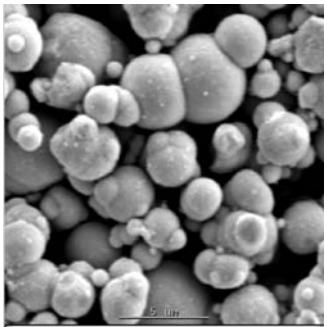

Fig. 3 Photo of iron powder under a scanning electronic microscope

$$I = \frac{\lambda^2}{8\pi^2} \cdot \frac{i_1 + i_2}{x^2} I_0, \tag{1}$$

where λ is the wavelength of the incident light; i_1 is the light intensity that the vibration is vertical to the plane of the incident light and the scattered light; i_2 is the light intensity that the vibration is parallel to the plane of the incident light and the scattered light.

What we should point out is that, according to the experimental results, the laser scattering is not in isotropism [33,34], but shows a strong forward tendency (as shown in Fig. 4).

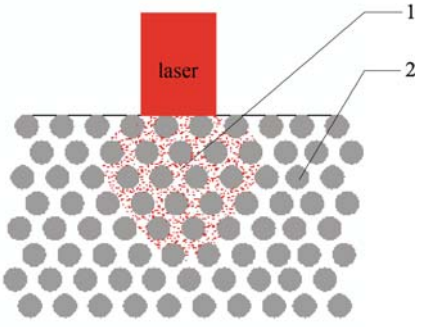

Fig. 4 Diagrammatic sketch of laser transmitting in powder (1. laser action area directly brings on powder to melt; 2. un-melted granules)

When the powder is being partly melted, the laser seldom scatters in the powder, and the non-melted granules remain in the original state shown in Fig. 3. So the granules of the microcosmic irregular array form up to millions of capillary holes and tubes, which generate capillarity to the liquid metal [7,9,35–38].

The formula of the infiltrating power goes as

$$\Delta p = \Delta p_1 + \Delta p_2 + \Delta p_3, \tag{2}$$

where Δp_1 is the capillary force; Δp_2 is the liquid phase

pressure; Δp_3 is the external pressure, such as the impact of the laser.

We believe that there is a "self-melting effect" of powder. As shown in Fig. 4, the area 1 is the laser action area that directly brings on powder to melt. In Fig. 5, this area is the first melting part under the laser action, and the arrow shows the expanding direction of the molt pool. It can be seen that owing to the laser scattering, the directly affected powder area enlarged (compared with the laser beam spot), so that the first melting area is no longer restricted to the beam spot scope. Then the infiltration caused by the capillary tube forces the heated liquid metal to flow sidewards and downwards. Meanwhile, those granules can also shift to the center, so there come the phenomena of the unevenly distributed material in the center and both sides, and the un-melted and semi-fused granules in area 1 of Fig. 4. It also determines the dimension of the final fabrication (thickness of the wall).

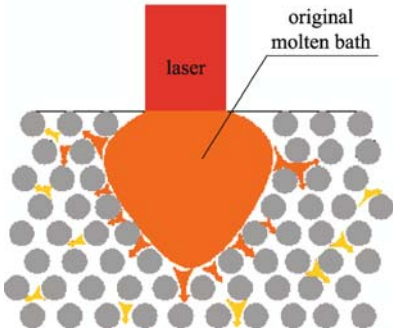

Fig. 5 Diagrammatic sketch of infiltration

In fact, the process occurred in the experiment is much more complicated. The interactions, which can play a great role to the final fabrication, existed not only between solid and liquid, but also gas. If the laser power density is high enough, some metal granules will be gasified, and the protecting gas will also have great affection to the final result. With the action of capillarity, these two parts of gas together with the melted powder and un-melted powder form a three-phase restrained flow system.

4 Results and future work

On balance, for this direct fusion of metal powder by a moving laser, the limit of accuracy is about 127 μm. Restrained by the accuracy of the current technology, the machining products would only reach the expected goal with some postprocessing. To overcome this limit, the focus of the powder machining in the future should be how to obtain thinner powder line, or even to arrange the granules in a string, and this technique could factually complete the direct laser machining. Therefore, it requires further research on this aspect.

Acknowledgements This work was supported by the National Basic Research Program of China (No. 2006CB605206).

References

1. Greul M, Pintat T, Greulich M. Rapid prototyping of functional metallic parts. Computers in Industry, 1995, 28(1): 23–28
2. Wu G H, Langrana N A, Sadanji R, Danforth S. Solid freeform fabrication of metal components using fused deposition of metals. Materials and Design, 2002, 23(1): 97–105
3. Das S, Wohlert M, Beaman J J, Bourell D L. Producing metal parts with selective laser sintering/hot isostatic pressing. JOM Journal of The Minerals, Metals and Materials Society, 1998, 50(12): 17–20
4. Exner H, Regenfuss P, Hartwig L, Klötzer S, Ebert R. Selective laser micro sintering with a novel process. Proceedings of SPIE, 2003, 5063: 145–151
5. Casalino G, De Filippis L A C, Ludovico A D, Tricarico L. An investigation of rapid prototyping of sand casting molds by selective laser sintering. Journal of Laser Applications, 2002, 14(2): 100–106
6. Ning Y, Wong Y S, Fuh J Y H, Loh H T. An approach to minimize build errors in direct metal laser sintering. IEEE Transactions on Automation Science Engineering, 2006, 3(1): 73–80
7. Kumar S, Kruth J P. Effect of bronze infiltration into laser sintered metallic parts. Materials and Design, 2007, 28(2): 400–407
8. Lanzetta M, Sachs E. Improved surface finish in 3D printing. Rapid Prototyping Journal, 2003, 9(3): 157–166
9. Sercombe T B, Schaffer G B. Rapid manufacturing of aluminum components. Science, 2003, 301(5637): 1225–1227
10. Liu J H, Shi Y S, Lu Z L, Xu Y, Chen K H, Huang S H. Manufacturing metal parts via indirect SLS of composite elemental powders. Materials Science and Engineering A, 2007, 444(1–2): 146–152
11. Dück J, Niebling F, Neeβe T, Otto A. Infiltration as post-processing of laser sintered metal parts. Powder Technology, 2004, 145(1): 62–68
12. Wu C M L, Han G W. Synthesis of an Al_2O_3/Al co-continuous composite by reactive melt infiltration. Materials Characterization, 2007, 58(5): 416–422
13. Maeda K, Childs T H C. Laser sintering (SLS) of hard metal powders for abrasion resistant coatings. Journal of Materials Processing Technology, 2004, 149(1–3): 609–615
14. Kruth J P, Mercelis P, Van Vaerenbergh J, Froyen L, Rombouts M. Binding mechanisms in selective laser sintering and selective laser melting. Rapid prototyping Journal, 2005, 11(1): 26–36
15. Kruth J P, Froyen L, Van Vaerenbergh J, Mercelis P, Rombouts M, Lauwers B. Selective laser melting of iron-based powder. Journal of Materials Processing Technology, 2004, 149(1–3): 616–622
16. Brandner J J, Hansjosten E, Anurjew E, Pfleging W, Schubert K. Microstructure devices generation by selective laser melting. Proceedings of SPIE, 2007, 6459: 645911
17. Sun M, Lü L, Fuh J Y H. Microstructure and properties of Fe-base alloy fabricated using selective laser melting. Proceedings of SPIE, 2002, 4426: 139–142
18. Santos E, Osakada K, Shiomi M, Morita M, Abe F. Fabrication of titanium dental implants by selective laser melting. Proceedings of

SPIE, 2004, 5662: 268–273
19. Lewis G K, Schlienger E. Practical considerations and capabilities for laser assisted direct metal deposition. Materials and Design, 2000, 21(4): 417–423
20. Vasinonta A, Beuth J L, Griffith M. Process maps for predicting residual stress and melt pool size in the laser-based fabrication of thin-walled structures. Journal of Manufacturing Science and Engineering, 2007, 129(1): 101–109
21. Milewski J O, Lewis G K, Thoma D J, Keel G I, Nemec R B, Reinert R A. Directed light fabrication of a solid metal hemisphere using 5-axis powder deposition. Journal of Materials Processing Technology, 1998, 75(1–3): 165–172
22. Syed W U H, Pinkerton A J, Lin L. Simultaneous wire- and powder-feed direct metal deposition: an investigation of the process characteristics and comparison with single-feed methods. Journal of Laser Applications, 2006, 18(1): 65–72
23. Qi H, Mazumder J, Green L, Herrit G. Laser beam analysis in direct metal deposition process. Journal of Laser Applications, 2005, 17 (3): 136–143
24. He X, Mazumder J. Transport phenomena during direct metal deposition. Journal of Applied Physics, 2007, 101(5): 053113
25. Alimardani M, Toyserkani E, Huissoon J P. Three-dimensional numerical approach for geometrical prediction of multilayer laser solid freeform fabrication process. Journal of Laser Applications, 2007, 19(1): 14–25
26. Wang X B, Chen J M, Jiao D M, Wu Q, Li G, Zuo T C. The beam characteristic of Nd:YAG frequency doubling in a KTP crystal by the resonant external ring cavity. Proceedings of SPIE, 2004, 5646: 636–642
27. Mie G. Beiträge zur optik trüber medien, speziell kolloidaler metallösungen. Annalen Der Physik, 1908, 25: 377–445
28. Penndorf R. Tables of the refractive index for standard air and the rayleigh scattering coefficient for the spectral region between 0.2 and 20.0 μ and their application to atmospheric optics. Journal of the Optical Society of America, 1957, 47(2): 176–182
29. Sudiarta I W, Chylek P. Mie-scattering formalism for spherical particles embedded in an absorbing medium. Journal of the Optical Society of America A, 2001, 18(6): 1275–1278
30. Du H. Mie-scattering calculation. Applied Optics, 2004, 43(9): 1951–1956
31. Yang W. Improved recursive algorithm for light scattering by a multilayered sphere. Applied Optics, 2003, 42(9): 1710–1720
32. Siu G G, Cheng L. Mie solution of light scattering from spheres of radii up to 80λ with digit-array method. Journal of the Optical Society of America B, 2002, 19(8): 1922–1929
33. Stout B, Nevière M, Popov E. *T* matrix of the homogeneous anisotropic sphere: applications to orientation-averaged resonant scattering. Journal of the Optical Society of America A, 2007, 24(4): 1120–1130
34. Gusarov A V, Kruth J P. Modelling of radiation transfer in metallic powders at laser treatment. International Journal of Heat and Mass Transfer, 2005, 48(16): 3423–3434
35. Kernan B D, Sachs E M, Allen S M, Sachs C, Raffenbeul L, Pettavino A, Lorenz A. Homogenous steel infiltration. Metallurgical and Materials Transactions A, 2005, 36(10): 2815–2827
36. Qin Z K, Yu J K, Zhang X Y. Infiltration kinetics of pressureless infiltration in SiCp/Al composites. Transactions of Nonferrous Metals Society of China, 2005, 15(2): 371–374
37. Sohn H, Yang D Y. Drop-on-demand deposition of superheated metal droplets for selective infiltration manufacturing. Materials Science and Engineering A, 2005, 392(1–2): 415–421
38. Ambrosi D. Infiltration through deformable porous media. Zeitschrift für Angewandte Mathematik und Mechanik, 2002, 82(2): 115–124